Published in final edited form as:
J Mol Biol. 2012 February 17; 416(2): 271–286. doi:10.1016/j.jmb.2011.12.045.

Crystal Structure and Regulation Mechanisms of the CyaB Adenylyl Cyclase from the Human Pathogen *Pseudomonas aeruginosa*

Hüsnü Topal[1], **Nanette B. Fulcher**[2], **Jacob Bitterman**[3], **Eric Salazar**[3], **Jochen Buck**[3], **Lonny R. Levin**[3], **Martin J. Cann**[4], **Matthew C. Wolfgang**[2,5], and **Clemens Steegborn**[6,*]

[1]Department of Physiological Chemistry, Ruhr-University Bochum, Germany

[2]Cystic Fibrosis/Pulmonary Research and Treatment Center, University of North Carolina, Chapel Hill, North Carolina, USA

[3]Department of Pharmacology, Weill Medical College of Cornell University, New York, USA

[4]School of Biological and Biomedical Sciences, Durham University, United Kingdom

[5]Department of Microbiology and Immunology, University of North Carolina, Chapel Hill, North Carolina, USA

[6]Department of Biochemistry, University of Bayreuth, Germany

Abstract

Pseudomonas aeruginosa is an opportunistic bacterial pathogen and major cause of healthcare-associated infections. While the organism's intrinsic and acquired resistance to most antibiotics hinders treatment of *P. aeruginosa* infections, the regulatory networks controlling its virulence provide novel targets for drug development. CyaB, a key regulator of *P. aeruginosa* virulence, belongs to the Class III adenylyl cyclase (AC) family of enzymes that synthesize the second messenger cyclic adenosine 3′,5′-monophosphate (cAMP). These enzymes consist of a conserved catalytic domain fused to one or more regulatory domains. We describe here the biochemical and structural characterization of CyaB and its inhibition by small molecules. We show that CyaB belongs to the Class IIIb subfamily and, like other subfamily members, its activity is stimulated by inorganic carbon. CyaB is also regulated by its N-terminal MASE2 domain, which acts as a membrane anchor. Using a genetic screen, we identified activating mutations in CyaB. By solving the crystal structure of the CyaB catalytic domain, we rationalized the effects of these mutations and propose that CyaB employs regulatory mechanisms similar to other Class III ACs. The CyaB structure further indicates subtle differences compared to other Class III ACs in both the active and inhibitor binding pocket. Consistent with these differences, we observed a unique inhibition profile, including identification of a CyaB selective compound. Overall, our results reveal mechanistic details of the physiological and pharmacological regulation of CyaB and provide the basis for its exploitation as a therapeutic drug target.

*Correspondence should be addressed to: Clemens Steegborn, University of Bayreuth, Dept. of Biochemistry, Universitätsstr. 30, 95447 Bayreuth, Germany; phone: (49)(921)552421; fax: (49)(921)552432; Clemens.Steegborn@uni-bayreuth.de.

ACCESSION NUMBERS: Coordinates and structure factors for the crystalstructure of CyaB have been deposited with the Protein Data Bank under accession code 3R5G.

Keywords

Class III; adenylyl cyclase; inhibition; activation; regulation mechanism

INTRODUCTION

Pseudomonas aeruginosa is a common cause of nosocomial and community-acquired pneumonia, and the primary cause of mortality in individuals with cystic fibrosis [1; 2]. Treatment of *P. aeruginosa* infections is handicapped by the bacterium's high intrinsic and acquired antibiotic resistance [3], which has left few effective treatment options [4]. The regulatory networks controlling *P. aeruginosa* virulence gene expression represent novel targets for drug development. Multiple *P. aeruginosa* virulence systems are controlled by the second messenger cyclic adenosine 3′, 5′-monophosphate (cAMP) via the cAMP-dependent global transcriptional regulator Vfr [5; 6; 7]. cAMP is formed by adenylyl cyclase (AC), and *P. aeruginosa* has three such enzymes. ACs can be grouped into six evolutionary distinct classes [8; 9]. *P. aeruginosa* ExoY belongs to Class II [10], a small group of secreted bacterial ACs that act as toxins. The two other *P. aeruginosa* ACs, CyaA and CyaB, belong to Class I and III, respectively. Class I enzymes are found exclusively in bacteria and are best known for their role in regulating nutrient utilization [8]. As yet, the role of *P. aeruginosa* CyaA is unknown. Class III is the largest family, which comprises members in almost all organisms including all mammalian ACs and guanylyl cyclases (GCs). Class III ACs have diverse cellular functions, including regulation of virulence mechanisms in several microbial pathogens. In *P. aeruginosa*, CyaB activity indeed accounts for the majority of intracellular cAMP and only CyaB is essential for *P. aeruginosa* colonization and dissemination in a mouse model of acute pneumonia [11]. CyaB activity appears to be triggered by environmental signals and we recently showed that CyaB is regulated by the Chp chemotaxis-like chemosensing system [12]; however, the exact environmental trigger and activation mechanisms remain to be identified.

Class III ACs possess one or more regulatory domains fused to the AC catalytic domain [13; 14]. Two catalytic domains, either from two polypeptides or from a single protein chain, form a (pseudo)dimeric C_1C_2 catalytic core. A variety of Class III crystal structures [15; 16; 17; 18] demonstrate that both monomers contribute conserved catalytic residues to the two active sites at the dimer interface. Two catalytic Mg^{2+} ions are co-ordinated by two Asp residues from C_1, and the transition state is stabilised by an Asp-Arg pair from C_2[9; 19]. Nucleotide specificity is primarily determined by a Lys from C_1 and an Asp from C_2, which bind to the ATP base [9; 18]. CyaB belongs to the Class III subgroup IIIb [20], where this Asp is exchanged for a Thr. This feature appears to correlate with sensitivity to inorganic carbon; i.e., the constituents of dissolved carbon dioxide (CO_2), including bicarbonate (HCO_3^-), carbonic acid, and carbonate (from now on referred to as CO_2/HCO_3^-). Stimulation by CO_2/HCO_3^- was first reported for the catalytic core of mammalian soluble adenylyl cyclase (sAC), and subsequently for catalytic domains of other, microbial "sAC-like" IIIb enzymes [16; 21; 22]. Although CO_2/HCO_3^- activation is unique for "sAC"-like ACs, the molecular mechanisms involved are assumed to share similarities with regulation by other stimuli, such as G-proteins or pH, and to be based on the relative rotation of catalytic domains and transitions between open and closed active site conformations[15; 16; 23].

In CyaB, the catalytic domain is fused to an N-terminal MASE2 (membrane associated sensor 2) domain [24]. MASE2 is a predicted transmembrane module found in a limited number of bacterial Class III ACs and diguanylyl cyclases. MASE2 domains are assumed to serve as sensors for environmental signals, relaying the signal to the cytosol by regulating

the activity of the fused catalytic domain. However, the exact roles of MASE2 domains in general and in CyaB in particular remain to be revealed.

Their role in virulence regulation renders microbial ACs interesting drug targets. In the fungal pathogen *Cryptococcus neoformans*, a CO_2-sensing AC regulates virulence, and interfering with this system prevents virulent growth [25; 26]. Interestingly, the regulation of Class IIIb ACs correlates with the sensitivity to established AC inhibitors: Class IIIb enzymes are sensitive to the synthetic compounds KH7 and BCC2/8, whereas other Class III ACs show a higher sensitivity to so-called P-site inhibitors, nucleotide derivatives which block the substrate binding pocket [9; 27; 28; 29]. It thus appears that specific inhibition of microbial ACs can be achieved and insights into the molecular details of the physiological and pharmacological regulation of such enzymes are an important step toward anti-infective compounds with novel mechanisms of action.

Here, we describe the biochemical and structural characterization of CyaB from *P. aeruginosa*. We determined that the MASE2 domain is required for significant catalytic activity *in vivo* and anchors the catalytic domain to the cytoplasmic membrane. We identified CyaB residues involved in the regulation of AC activity using a random mutagenesis strategy and gain-of-function screen, and solved the crystal structure of the CyaB catalytic domain to analyze the location and function of these residues. We further describe the modulation of CyaB through CO_2/HCO_3^- and known AC inhibitors. Our results are a first step toward understanding the physiological regulation of CyaB and to exploit it as a drug target.

RESULTS

The CyaB N-terminal region controls catalytic activity

P. aeruginosa CyaB (UniProt Q9HZ23) regulates virulence factor expression and has been implicated in coupling this process to environmental signals [12]. Importantly, a *P. aeruginosa cyaB* mutant is attenuated in a mouse pneumonia model [11]. Because these observations suggest that the enzyme may serve as a drug target, we set out to study its physiological and pharmacological regulation. We previously showed that the C-terminal AC homology region of CyaB has catalytic activity *in vitro* [12]; we now explored whether regions outside the catalytic domain play a role in CyaB activation. We investigated how AC activity is affected by i) the extreme N-terminal segment, which is basic, proline-rich, and predicted to be cytoplasmically exposed and ii) the putative MASE2 sensing domain, which contains multiple transmembrane segments (Figure 1a). We constructed *cyaB* alleles in which nucleotides corresponding to the first 17 amino acids ($cyaB_{\Delta 1–17}$) or the MASE2 domain ($cyaB_{\Delta 1–216}$) were deleted. The mutant *cyaB* alleles encoding $CyaB_{\Delta 1–17}$ and $CyaB_{\Delta 1–216}$ were expressed from plasmids under the control of the IPTG-inducible *tac* promoter.

We assessed catalytic activity using a cAMP-dependent reporter gene (*lac*P1Δ*lacI-lacZ*) based on the *Escherichia coli lac*P1 promoter, which was previously shown to reflect intracellular cAMP levels in *P. aeruginosa* [30]. Plasmid-borne *cyaB* alleles were transferred to *P. aeruginosa* strain PAK lacking both chromosomally encoded adenylyl cyclases (*cyaA* and *cyaB*) and harboring the *lac*P1Δ*lacI-lacZ* reporter in the vacant φCTX phage integration site on the chromosome. We determined the induction conditions (IPTG concentration) under which the plasmid-encoded CyaB proteins (wild-type and truncated forms) were expressed at levels roughly equivalent to native CyaB in the wild-type strain as assessed by immunoblotting bacterial lysates with anti-CyaB antibody generated against a synthetic peptide corresponding to the extreme C-terminal portion of CyaB (Figure 1b). We then assessed cAMP reporter activity under these conditions, correcting for minor differences in protein levels based on quantitative analysis of CyaB immunoblots (Figure 1c). Wild-type

CyaB, but not $CyaB_{\Delta 1–17}$ or $CyaB_{\Delta 1–216}$, restored wild-type reporter activity in PAK*cyaAB::lac*P1Δ*lacI-lacZ*, with $CyaB_{\Delta 1–216}$ displaying a more dramatic reduction in reporter activity than $CyaB_{\Delta 1–17}$. These results indicate that both the truncated proteins have reduced activity relative to full-length CyaB. This finding, combined with the observation that the CyaB catalytic domain has activity *in vitro* [12], suggests that the CyaB catalytic domain retains function but that the N-terminal non-catalytic domain is required for full activity *in vivo*. Overall, our results indicate that both the putative cytoplasmically exposed N-terminal segment and the MASE2 domain influence CyaB AC activity *in vivo*.

Because CyaB is predicted to be an integral cytoplasmic membrane protein, we explored the possibility that $CyaB_{\Delta 1–17}$ and/or $CyaB_{\Delta 1–216}$ are less active *in vivo* due to altered subcellular localization. To determine the localization of CyaB, $CyaB_{\Delta 1–17}$, and $CyaB_{\Delta 1–216}$ within *P. aeruginosa*, we prepared fractions containing soluble (periplasmic and cytoplasmic) and insoluble (total membrane) proteins from PAK expressing the corresponding proteins. We then separated the total membrane fraction into inner and outer membrane fractions by sarkosyl solubilization. An equivalent amount of each fraction was analyzed by immunoblotting to detect CyaB, the cytoplasmic RNA polymerase (RNAP) beta subunit [31], the inner membrane protein SecY, or the outer membrane protein OprF[32]. Full-length CyaB and $CyaB_{\Delta 1–17}$ were detected exclusively in the total membrane and inner membrane fractions, whereas $CyaB_{\Delta 1–216}$ was present only in the soluble cytoplasm-periplasm fraction (Figure 2). These results demonstrate that CyaB is localized to the inner membrane of *P. aeruginosa* and that localization is MASE2-dependent. In addition, the fact that CyaB and $CyaB_{\Delta 1–17}$ showed no difference in subcellular localization suggests that the reduced activity of $CyaB_{\Delta 1–17}$ is not due to improper targeting. Taken together, these results reveal that both the extreme N-terminal segment and the putative MASE2 sensing domain influence CyaB activity; the MASE2 domain functions in proper subcellular targeting, and the N-terminal segment contributes in an as yet undefined way. It remains to be shown whether these effect on CyaB activity are static or whether they contribute to physiological CyaB regulation mechanisms.

Identification of CyaB residues involved in enzyme activation

We next sought to identify CyaB residues critical for catalytic activation. We conducted a screen for CyaB mutants with elevated activity using the *lac*P1Δ*lacI-lacZ* reporter for cAMP production. To enhance differences between the parent strain and mutants with elevated CyaB activity, we performed the screen in a strain lacking PilG, a Chp chemosensing system component that activates CyaB [12]. Plasmid-based expression of wild-type levels of CyaB in a *cyaABpilG* mutant does not complement reporter activity [12], leading to colonies that are less blue on X-gal plates (data not shown). To identify *cyaB* mutations resulting in elevated AC activity, we screened for suppressors of this *pilG* phenotype. We generated a library of random substitution mutations in plasmid-borne *cyaB* (pMMBV2-*cyaB*) by PCR mutagenesis and screened it in PAK*cyaABpilG* on X-gal plates under conditions that yielded wild-type CyaB levels. To identify the *cyaB* lesions, we transferred the pMMBV2-*cyaB* plasmids from darker colonies to *E. coli* DH5α, isolated plasmid DNA and sequenced *cyaB*. We identified 28 *cyaB* clones harboring single missense mutations representing 10 unique sites within CyaB (Table I): two in the linker region, six in the catalytic domain and two in the C-terminal tail (Figure 3a). We then transferred a representative clone harboring each unique mutation into PAK*cyaAB* to assess cAMP reporter activity. Due to saturation effects, the *lac*P1Δ*lacI-lacZ* reporter does not accurately reflect cAMP concentrations above wild-type level [12; 30]. Therefore, we assayed the CyaB mutants in low salt media (5 mM versus 200 mM NaCl), a condition that results in reduced intracellular cAMP accumulation [33]. To determine the effect of salt concentration on reporter activity, we assayed PAK::*lac*P1Δ*lacI-lacZ* in LB medium containing 5 mM or 200 mM NaCl and observed that reporter activity

under high–salt medium is about 2.3-fold higher than in low-salt medium (Supplementary Figure S1). We then assayed cAMP reporter activity of the CyaB mutants expressed in PAK*cyaAB::lac*P1Δ*lacI-lacZ* under low-salt conditions. Although the strains were expressed under identical induction conditions (50 μM IPTG), we examined CyaB levels by quantitative immunoblot to address the possibility that the point mutations altered protein stability. CyaB mutant protein levels were roughly comparable to that of wild-type CyaB and to adjust for the subtle differences observed, we normalized reporter activity to CyaB levels. The majority of CyaB mutants had significantly elevated cAMP reporter activity (greater than fourfold) compared to that of wild-type CyaB expressed in the *cyaAB* mutant ($P \leq 0.043$) (Figure 3b). The activity of the R412H mutant was also elevated, but the increase was not statistically significant. We also transferred a *cyaB* wild-type plasmid from the *cyaABpilG* screening strain to PAK*cyaAB*, yielding equivalent activity to PAK*cyaAB* expressing pMMBV2-*cyaB*. We thus conclude that the increased activity displayed by the mutants is due to its nucleotide substitution in *cyaB* and the resulting change of a CyaB protein residue, suggesting that enzyme activation is controlled by specific regions both within and outside of the catalytic domain.

Crystal structure of the CyaB catalytic domain

In order to interpret data on the physiological (see above) and pharmacological (see below) regulation of CyaB, we solved the crystal structure of the *P. aeruginosa* CyaB catalytic domain. The enzymatically active CyaB catalytic core, comprised of residues 220–416 ($CyaB_{220–416}$), was produced in *E. coli* and the homodimeric CyaB protein obtained from purification was crystallized. The CyaB structure was then solved using Patterson search techniques with the AC homodimer of CyaC from *Spirulina platensis* [16] as a search model, and it was refined at 1.5 Å resolution to R_{cryst} and R_{free} values of 18.6 % and 23.0 %, respectively (Table II). The final CyaB model comprises residues 222–416 of two monomers, A and B, in the asymmetric unit, with no residues in the disallowed region of the Ramachandran plot and 99 % of the residues in the most favourable areas.

The overall structure of CyaB (Figure 4a,b) shows, besides small deviations in detail, the general architecture of Class III AC enzymes [9; 17; 18]. Each monomer contains a central seven-stranded β-sheet, shielded from solvent by α-helices(Figure 4a). The β-strands β1 to β4 form a βαββαβ arrangement, and a two-stranded β sheet formed by β5 and extensions of β4 protrude from the core of the domain. This small sheet interacts with β2 and β3 of the partner monomer to form the wreath-like, catalytically active dimer (Figure 4b). Two active sites are formed at the dimer interface, employing substrate binding and catalytic residues from both monomers (Figure 4c).

CyaB more closely resembles the “closed” conformation of CyaC, which presumably approximates a product complex, as opposed to the “open” conformation likely representing the apo form before substrate binding (Figure 4d) [16]. Thus, we expect the observed CyaB conformation needs to open up to allow entry of the substrate, which would explain why no substrate analog was visible in the active site after soaking experiments (data not shown). Substrate analog cocrystallization attempts also resulted in apoenzyme crystals, which could indicate that the observed, closed CyaB conformation crystallizes preferentially. Comparison of the CyaB active site with the two CyaC conformations reveals that all residues important for substrate binding and catalysis are in similar positions; however, several showed substantial differences in their conformation. In particular, one of the two conserved Asp residues responsible for binding the divalent metal ions, which in turn bind to the substrate phosphates, is turned away from the ion positions (Asp234; Figure 4e). In contrast to the active site entrance, this state appears like an open state, ready to accommodate the metal ions, similar to one of two sites in the Class III GC Cya2[18]. Similar to Cya2, the catalytic dimer shows asymmetry, which might indicate that both active sites

are in different states. This observation could even hint at half-of-the-sites activity, i.e. one active site being in a catalytically active state is coupled to the second one being in an inactive conformation, which was previously observed for other Class III cyclases [18; 34].

Structural implications for CyaB activation

The residues implicated in CyaB activation are highlighted in the crystal structure of the CyaB catalytic domain in Figure 5a,b. The N- and C-terminal extensions of the CyaB core crystallized here show similarities to corresponding regions in other AC enzymes, but they have not been functionally or structurally characterized and were therefore omitted from our analysis. It should be noted, however, that the activating mutations in C-terminus and linker might indicate regulatory functions for these regions (although static effects cannot be excluded – see above) and the MASE2 domain connected to the linker.

The most N-terminal activating mutation identified in the genetic screen (above), Arg318Trp, affects a residue in the C-terminus of α3 on the surface of the catalytic core, oriented toward the solvent (Figure 5a,b). Interestingly, the corresponding region of the mammalian transmembrane ACs (tmACs) serves as a binding site for the regulatory heterotrimeric G-protein subunit $G_s\alpha$ [15], and most likely $G_i\alpha$ [35]. Binding of G-protein subunits is predicted to regulate tmAC activity by influencing the relative orientation of the catalytic domains. The activating effect of changing Arg to a large, hydrophobic Trp might indicate that within the full-length CyaB protein, this area is shielded from solvent and thus also contributes to a regulatory interaction interface. However, the C-terminus of helix α3 and the connected loop show significant variations in length and sequence between the sAC-like and tmAC families [9], and Arg318 is not conserved in other sAC-like ACs. Therefore, Arg318 may mediate regulation by a CyaB-specific partner domain that is either part of full-length CyaB (e.g., the MASE2 domain) or a separate regulatory protein. Interfering with this regulatory interaction may be an attractive approach for drug development. It is tempting to speculate that this protein region generally plays a role in adapting individual Class III ACs to their specific regulators.

Several of the identified activating mutations affect positions involved in interactions with two structural elements that undergo major conformational changes during the catalytic cycle, the α1 helix and the β7/β8 loop [9]. The mutations Leu326Pro (Figure 5a) and Phe399Ile/His are also close to putative substrate binding residues (Arg329 and Lys397, respectively) and could have direct effects on the local protein conformation, but their roles in packing interactions seem more obvious explanations for the activating effects. Leu326Pro affects the hydrophobic interface formed by the N-terminus of β4, the Arg318-carrying α3 discussed above, and the flexible helix α1, which has to move toward the dimer center [9; 36], either upon substrate binding [19] or substrate conversion [16]. The mutation might make α1 more flexible due to less tight packing, which would facilitate active site closure or its induction through modulator binding. In contrast to Arg318Trp, which likely affects CyaB activity only in presence of a partner domain or protein (see above), the Leu326Pro mutation would be expected to directly increase specific activity of the isolated catalytic domain. We therefore generated this single site variant, $CyaB_{220–416}$-Leu326Pro, and compared its specific activity to wildtype $CyaB_{220–416}$. Consistent with the proposed facilitating effect on the catalytic β7/β8 movement, the Leu326Pro mutation indeed increased specific activity due to significantly faster substrate turnover, whereas the substrate affinity was comparable to wildtype $CyaB_{220–416}$ (Figure 5b). Similarly to Leu326, residue Phe399, which was substituted with either His or Ile, resides in the β7/β8-loop that moves, together with α1, during catalysis, thereby repositioning the phosphate-binding residue Lys380. Exchange of the phenylalanine to a smaller (Ile) or less hydrophobic (His) residue should weaken the packing of this loop against α4 and thereby make it easier for the loop to move. The Glu377Gly mutation in α5 appears mainly solvent exposed in the closed

conformation seen in the CyaB structure, but it might contribute to interactions to the β7/β8-loop, similar to Phe399, in more open conformations. Although an increase in CyaB activity due to the Arg412His mutation did not achieve statistical significance in our analysis, the fact that this mutant was identified in our screen suggests this residue may still play a role in enzyme activation. The mutation Arg412His affects a region opposite from the active site, on the outside of the dimer and might thus influence interactions with regulatory partners (domains or proteins), but its position at the base of the β7/β8 arm indicates that its effect might again be based on influencing the movement of β7/β8. In contrast, the mutation Ile352Thr affects a position not contacting β7/β8, but involved in packing β5 and α4 (Figure 4a,b; Figure 5a). This residue is located next to Thr351, which recognizes the substrate base (Figure 4c) and likely needs to rearrange during transition state formation. We assume the neighbouring residue influences these rearrangements through packing interactions that modulate the backbone flexibility of this region.

While these hypothesized roles for the identified residues are consistent with our knowledge on general mechanisms of Class III catalysis and regulation, they reveal mechanistic differences from other Class III ACs, such as the one involving Arg318, suggesting that interfering with these mechanisms should yield highly specific drugs.

CyaB belongs to the inorganic carbon-responsive family of sAC-like enzymes

Based on key active site polymorphisms, CyaB is assigned to the Class IIIb ACs, whose members are characterized by responsiveness to CO_2/HCO_3^- [9; 22]. To examine the response of $CyaB_{217–463}$ to CO_2/HCO_3^-, it was necessary to first determine its divalent metal ion requirement and responsiveness to pH. $CyaB_{217–463}$ activity was significantly higher in the presence of Mn^{2+}-ATP compared to Mg^{2+}-ATP as substrate (Figure 6; note differences in scale), as observed for most Class III ACs. In presence of either Mg^{2+}-ATP or Mn^{2+}-ATP, $CyaB_{217–463}$ activity increased with pH values ranging from 6.5 to 8.5 (Figure 6a). CO_2/HCO_3^- stimulated $CyaB_{217–463}$ activity in the presence of either divalent, with optimal stimulation occurring at pH 7.5 (Figure 6a). As Mn^{2+}-ATP at pH 7.5 supported both optimal specific activity and CO_2/HCO_3^- dependent enzyme stimulation, further analysis was performed under these conditions. Stimulation of specific enzyme activity was cation independent (Figure 6b), and maximal stimulation occurred at 50 mM salt (Figure 6c). We were unable to calculate an accurate EC_{50} because activity dropped precipitously at concentrations >50 mM HCO_3^- presumably due to HCO_3^--dependent precipitation of the essential divalent cation. However, we were able to conclude that stimulation occurs over physiologically relevant CO_2/HCO_3^- concentrations (typically 5 to 25 mM). 20 mM CO_2/HCO_3^- increased enzyme activity compared to Cl^- through an increase in enzyme turnover (k_{cat} of 3.8±0.2 min^{-1} and 1.2±0.1 min^{-1}, respectively [S.E.M., N=6]) consistent with other Class IIIb enzymes [22; 37]. We thus conclude that physiological concentrations of CO_2/HCO_3^- modulate CyaB activity. It remains to be determined in which physiological pathways this regulatory mechanism is employed.

Pharmacological inhibition of CyaB

CyaB might serve as target for novel antibiotics, and we therefore tested a number of known Class III AC inhibitors for their efficacy against purified enzyme. Catechol derivatives of estrogen (CE) were previously shown to be non-specific, noncompetitive inhibitors of Class III ACs [38]. Consistently, 2-hydroxy estradiol inhibited $CyaB_{220–416}$ significantly at 100 μM (Figure 7a). Previous crystallographic studies revealed that the catechol in CEs chelates the catalytic divalent metal ion, and that the hydrophobic steroid scaffold binds to a pocket present in all Class III cyclases, albeit with differences in the exact shape [38]. An overlay of CyaB with the CE complex of CyaC (Figure 7b) indeed shows the presence of an analogous pocket in CyaB. Using the CyaC/CE structure, we developed more specific ligands, BCC2

and BCC8, which specifically and potently inhibited CyaC and mammalian sAC, but not tmACs [29]. In CyaB, the CE binding pocket is slightly smaller, which might indicate that the bulkier compound BCC2 should not be able to bind efficiently. Indeed, 100 μM BCC2 only weakly inhibited CyaB activity (Figure 7a). This difference in BCC2 response among the Class IIIb ACs examined indicates that exploiting the CE binding site may be an approach enabling the development of specific inhibitors for individual ACs including CyaB.

All Class IIIb cyclases tested in our laboratories have been sensitive to the inhibitor KH7, which appears to be specific for sAC-like ACs [27] and whose mechanism of action is unknown. Surprisingly, the sAC-like enzyme CyaB was completely insensitive to KH7 at concentrations up to 100 μM. Despite this observation, we hypothesized that minor modifications of KH7 chemical space could yield effective inhibitors of CyaB. We therefore screened 57 KH7-related compounds that differed with respect to the functional groups attached to the KH7 acyl hydrazone backbone (Figure 7c,d). Several compounds increased the assay signal, and we will test in a separate study whether they are indeed CyaB activators, possibly employing the mechanism of the AC activator forskolin [9]. However, one of these compounds, KH7.148 (Figure 7d), inhibited CyaB activity with an IC_{50} of ~10 μM (Figure 7e). Interestingly, KH7.148 was the only KH7-like compound with a catechol moiety, and this shared chemical structure could indicate a mechanism of inhibition similar to that of catechol estrogens [38]. The steepness of the KH7.148 inhibition curve (Figure 7e) could indicate cooperativeness compatible with binding to the CE site, which is partly formed by the CE molecule bound to the second site of the AC dimer [38], but further experimental work is required to clarify the KH7.148 mechanism. Interestingly, KH7.148 is only a weak inhibitor of basal mammalian sAC activity, with an $IC_{50} > 100$ μM (Supplementary Figure S2), showing that KH7.148 is not a promiscuous inhibitor but shows selectivity even between these two closely related enzymes. These results indicate that it is possible to develop highly specific inhibitors of CyaB, an important step in exploiting this enzyme as a therapeutic target, and that KH7.148 can serve as a first lead compound. Furthermore, the CyaB structure described here provides a starting point for future structure-based drug development efforts.

DISCUSSION

The nucleotidyl cyclase Class III is a large family of proteins featuring a conserved catalytic domain architecture but exhibits significant sequence variation in most residues not directly involved in catalysis [9; 17]. Consistently, the catalytic domains respond to different signalling molecules, such as G-proteins, calmodulin, or CO_2/HCO_3^-. Additionally, each Class III AC catalytic domain is fused to unique regulatory domains [14], providing individual regulation for specific ACs. The molecular basis for AC regulation has been characterized for a few examples [39], and an emerging theme for AC regulation by different sensor domains and binding proteins is an induced relative rotation of the catalytic domains that optimizes the active site at the dimer interface [9; 15]. Our finding that the MASE2 domain of *P. aeruginosa* CyaB is required for membrane localization and full catalytic activity is consistent with a model in which MASE2 receives an activating signal and, in response, influences the relative rotation of the catalytic domains. Such a signaling function of MASE2 in CyaB is supported by the fact that the MASE2 domain is distinct from the membrane anchors present in other Class III ACs, but further experiments are needed to identify the factor(s) triggering MASE2. Our assessment of the regulatory regions of CyaB beyond the MASE2 domain also implicates the extreme N-terminal (cytosol-exposed) region of CyaB in catalytic regulation, but it is not clear whether this regulation is direct, via contact with the catalytic domain itself, or indirect, via inducing conformational alteration of MASE2 that in turn affects catalytic activity.

CyaB is required for production of multiple *P. aeruginosa* virulence factors including secreted toxins and type IV pili (tfp), which are surface fibers at the bacterial pole mediating adherence to host tissue and "twitching motility", a surface-associated motility that involves rapid cycles of pilus extension and retraction. CyaB is localized in the bacterial poles [40], a location shared by the tfp biogenesis machinery [41] and components of the Chp chemosensory system [40; 42]. We predict that the MASE2 domain, which we show here is required for inner membrane targeting, is also likely to be required for localization to the bacterial poles. The localization pattern of CyaB, in combination with our finding that CyaB catalytic activity is regulated by the Chp system [12], suggests the enzyme may be involved in coupling an unknown signal to functional output (tfp extension and retraction), possibly as part of a multi-protein complex anchored at the inner membrane. The Chp system complex consists of a histidine kinase, accessory factors, and soluble receiver proteins anchored to an inner membrane receptor (MCP). One intriguing possibility is that CyaB activity is controlled via interaction with Chp system regulatory domains. In support of this model are examples of Class III AC domains coupled to two-component kinase and receiver domains [14; 43], and the report that AC/chemotaxis MCP chimeras produce cAMP in response to the appropriate ligand [44]; it remains to be shown, however, whether Chp system regulation of CyaB is direct or indirect.

Although regulation by CO_2/HCO_3^- is a common feature of sAC-like ACs, this regulation has features specific for CyaB. For this AC, it is pH dependent with an optimum at 7.5 and is distinct from previous modes of regulation which were either optimal at acidic pH, e.g. Slr1991[37], or relatively pH independent, e.g. sAC [45]. As mentioned, select fungi utilize CO_2 to initiate a pathogenic response. An optimal pH of 7.5 for carbon regulation of CyaB might represent a mechanism by which the relatively high CO_2/HCO_3^- concentration in the eukaryotic host can increase cAMP accumulation and contribute to the organism's pathogenic lifestyle.

The ACs of microbial sensor systems regulating virulence factors are interesting drug targets. In two species of pathogenic fungi, *Candida albicans* and *C. neoformans*, a CO_2-sensing system based on a sAC-like AC and a carbonic anhydrase (CA) regulate virulent growth [25; 26; 46; 47]. Inhibition of CAs has been extensively studied, but despite some promising novel approaches such as using novel chelating groups for the CA catalytic zinc ion [48], it has proven difficult to develop compounds specific for the microbial enzyme but inactive against host CAs [26]. The fact that CyaB also responds to CO_2/HCO_3^- might indicate that a CA contributes to its regulation, but further studies will be needed to identify this or other CyaB regulators and the mechanisms they employ. The only option currently available to interfere with this *P. aeruginosa* system is direct inhibition of the CyaB catalytic domain. Specific inhibition of Class III ACs is challenging, but progress in recent years has stimulated efforts to exploit these proteins as drug targets [29; 49; 50]. Intriguingly, we find that the CyaB binding pocket for catechol estrogen and BCC2/8[29; 38] shows differences to those in other sAC-like enzymes. Thus far, these differences correlated with compound sensitivity suggesting that targeting this CyaB pocket is an attractive approach for developing specific drugs. Also of interest, the compound KH7, which was effective against all previously tested Class IIIb cyclases, is relatively inert towards CyaB. In contrast, a single catechol-containing KH7-derived compound (KH7.148) proved to be a potent, selective inhibitor of CyaB, indicating that this and other KH7 derivatives hold the potential to be developed into therapeutic drugs that exploit CyaB's role in virulence regulation. Mechanistic studies on AC inhibition by KH7-like compounds will be an important part of the efforts to develop AC-targeted therapeutics. Such efforts focused on *P. aeruginosa* should be complemented by further studies on the CyaB regulatory mechanisms described here.

MATERIALS AND METHODS

Plasmid and strain construction

Strains used in this study are listed in Supplementary Table S1. The *cyaB* alleles encoding truncated versions of CyaB (*cyaB*$_{\Delta 1–17}$ and *cyaB*$_{\Delta 1–216}$) for expression in *P. aeruginosa* correspond to CyaB amino acid positions 18–463 or 217–463, respectively (*cyaB*$_{\Delta 1–17}$ includes the existing methionine codon at position 18 whereas *cyaB*$_{\Delta 1–216}$ has an added methionine start codon). The expression plasmids pMMBV2-*cyaB*$_{\Delta 1–17}$ and pMMB-*cyaB*$_{\Delta 1–216}$ were made by PCR amplification using chromosomal DNA from *P. aeruginosa* strain PAK as template and either 5′ScyaB/3′PA3217 or 5′cyaB200/3′PA3217 oligonucleotide pairs, respectively (Supplementary Table S2). Amplified *cyaB*$_{\Delta 1–17}$ and *cyaB*$_{\Delta 1–216}$ fragments were cloned into pDONR201 by Gateway cloning (Invitrogen) and then transferred to pMMBV2GW or pMMBGW, respectively. All pMMB-derived plasmids were transferred to PAK*cyaAB::lac*P1Δ*lacI-lacZ* by triparental mating as described [51].

cAMP reporter assay and immunoblotting

β-galactosidase assays were performed as previously described [12] using bacteria grown in LB broth to mid-log growth phase (OD_{600} = 0.8). For the indicated assays, bacteria were grown in LB with 5 mM NaCl (low salt) or 200 mM NaCl (high salt). For CyaB immunoblot analysis, bacteria were normalized based on OD_{600} reading and pelleted by centrifugation for 2 minutes at 13,000 x g. To create whole-cell lysates, bacteria were suspended in 100 μl H_20 and treated with 1 μl DNaseI (10 mg/ml) for 10 minutes at 37°C. SDS/PAGE sample buffer (100 μl) was then added followed by incubation at 45°C for 45 minutes. Membranes were probed with affinity-purified antiserum against CyaB (1:5,000 dilution) and visualized by enhanced chemiluminescence as described [12]. For quantitative analysis of immunoblot autoradiographs, the signal intensity of bands corresponding to CyaB, CyaB$_{\Delta 1–17}$ or CyaB$_{\Delta 1–216}$ was determined by densitometry using ImageJ software (National Institutes of Health; rsbweb.nih.gov/ij/). To correct cAMP reporter activity values for CyaB protein levels, the signal density of each sample relative to that of the control (*cyaA* carrying empty vector or *cyaAB* carrying pMMBV2-*cyaB*) was determined and used to calculate “relative activity” [relative activity = β-galactosidase activity (Miller units)/ [sample signal density/control signal density]]. Calculations to assess statistical significance for relative activity values were made using an unpaired two-tailed *t*-test.

Bacterial fractionation

P. aeruginosa strains were grown in 500 ml LB broth with the indicated amount of isopropyl-β-thiogalactoside (IPTG) at 37°C for 2.5 h and harvested by centrifugation at 10,000 x g. Fractionation was conducted based on the protocol of Boyd and Lory [52]. Briefly, the pellets were resuspended in 4 ml of 50 mM Tris, pH 7.5, 10 mM $MgCl_2$ and treated with RNase I and DNase I (50 μg/ml) for 10 min. Bacteria were lysed by 2 passages through a French pressure cell (8000 lb/in^2). Phenylmethysulfonyl fluoride (PMSF) was added to 100 μg/ml, lysozyme was added to 0.5 mg/ml, and the solution was incubated at room temperature for 1 h. The lysate was centrifuged at 10,000 × g for 10 min to remove unlysed cells and the resulting supernatant was centrifuged at 100,000 × g for 1 h to create total membrane (pellet) and cytosol/periplasm (supernatant) fractions. The cytosol/periplasm fraction was subjected to a second round of centrifugation at 100,000 × g for 1 h. The total membrane fraction was suspended in 5 M urea, 100 mM Tris, pH 7.5 by passage through a 22-gauge needle to remove peripheral membrane proteins. The total membrane fraction was centrifuged at 100,000 × g for 1 h and then subjected to a second wash with 5 M urea, 100 mM Tris, pH 7.5. The total membrane fraction was suspended in phosphate buffered saline (PBS). Sarkosyl was added to 0.25 % and mixtures incubated on ice for 1 h and then centrifuged at 100,000 x g for 1 h. The sarkosyl-soluble (inner membrane) fraction was

subject to a second round of centrifugation at 100,000 × g. The sarkosyl-insoluble (outer membrane) fraction was suspended in PBS plus 0.25 % sarkosyl and centrifuged again at 100,000 × g for 1 h. The final outer membrane fraction was suspended in PBS by passage through a 22-gauge needle, centrifuged at 13,000 × g for 1 min to pellet debris and the supernatant was transferred to a new tube. Protein concentrations for membrane and cytosol/periplasm fractions were determined using BCA protein assay (Pierce). Samples for CyaB immunoblotting were solubilised in SDS/PAGE sample buffer at 45°C for 45 minutes; all other samples were solubilised at 95°C for 5 minutes. Samples were resolved by SDS/PAGE on 12 % (CyaB) or 7.5 % (RNA polymerase (RNAP), OprF, and SecY) acrylamide gels and transferred to nitrocellulose membranes. Immunoblots were probed with anti-CyaB antibody (1:5,000) [12], antiserum specific for OprF (1:20,000) or SecY (1:5000) ([32]; gift of George O'Toole), or antibody against *E. coli* RNAP β subunit (1:10,000; Neoclone). CyaB, OprF and SecY were detected with horseradish peroxidase (HRP)-conjugated goat anti-rabbit Ig (Jackson; 1:25,000); RNAP was detected with HRP-conjugated goat anti-mouse Ig (Jackson; 1:25,000). Immunoblots were developed using enhanced chemiluminescence reagents (Millipore) and visualized by autoradiography.

CyaB mutagenesis and screening

PCR mutagenesis of *cyaB* was performed using Taq DNA polymerase (Qiagen), $ATTB1^{start}$ and $ATTB2^{stop}$ oligonucleotides [7], 0.5 μM $MgCl_2$ and pMMBV2-*cyaB* as template. The pool of amplified products were cloned into pMMBV2[12] by Gateway cloning (Invitrogen) and transformed into *E. coli* DH5α. The plasmid library carrying mutagenized *cyaB* was transferred to PAK*cyaABpilG::lac*P1Δ*lacI-lacZ* by triparental mating. Dilutions of the bacteria were plated on LB agar plates containing 25 μg/ml irgasan, 150 μg/ml carbenicillin (carb), 40 μg/ml (X-gal) and 50 μg/ml IPTG. Colonies that appeared darker blue were selected from plates containing approximately 500 colonies. Candidate plasmids were recovered from *P. aeruginosa* by suspending the bacteria in water, incubating for 10 minutes at 95°C followed by centrifugation for 1 min. An aliquot of the resulting supernatant was transformed into *E. coli* DH5α, selecting on plates containing 30 μg/ml carb. pMMBV2-*cyaB* mutant plasmids were harvested from *E. coli* DH5α for sequencing and then transferred by triparental mating to PAK*cyaAB::lac*P1Δ*lacI-lacZ.*

The $CyaB_{220–416}$ mutant Leu326Pro was generated from the $CyaB_{220–416}$ wildtype expression construct (see below) using the QuickChange Lightning kit (Agilent), and the protein was expressed and purified as described for wildtype $CyaB_{220–416}$(see below).

Recombinant protein production and purification

Open reading frames corresponding to the catalytic domain of CyaB from *P. aeruginosa* strain PAK, with or without the C-terminal tail (residues 220–416 and 217–463 for $CyaB_{220–416}$ and $CyaB_{217–463}$, respectively), were cloned into pQE30 (Qiagen), resulting in an N-terminal His-tag with ($CyaB_{220–416}$) or without ($CyaB_{217–463}$) a TEV protease cleavage site. Constructs were expressed in *E. coli* SG13009[pREP4] and M15[pREP4] (Qiagen) in Luria-Bertani broth containing 100 μg/ml ampicillin and 50 μg/ml kanamycin for 18 h at 20°C after induction with 0.5 mM IPTG at an OD_{600} of 0.6. Harvested cells were resuspended in 50 mM Tris-HCl, pH 7, 200 mM NaCl, 3 mM DTT, 0.25 mM PMSF, treated with 0.2 mg/ml lysozyme for 15 min on ice, and disrupted in a French Press. Cleared lysate (50 min centrifugation at 50,000 x g and 4°C) was supplemented with 5 mM imidazole and allowed to bind to Ni-NTA agarose (Qiagen) for 1 h at 4°C. The resin was washed with 10 volumes of 50 mM Tris-HCl, pH 7, 400 mM NaCl, 10 mM imidazole, 2 mM DTT, and subsequently with 10 volumes of 50 mM Tris-HCl, pH 7, 200 mM NaCl, 15 mM imidazole, 2 mM DTT, and protein eluted with TEV protease overnight at 4°C ($CyaB_{220–416}$) or 10 volumes of 50 mM Tris-HCl, pH 7, 200 mM NaCl, 150 mM imidazole, 2 mM DTT

($CyaB_{217–463}$). Cleaved $CyaB_{220–416}$ protein was eluted in 50 mM Tris-HCl, pH 7, 150 mM NaCl, 2 mM DTT and concentrated in a 10 kDa Amicon concentrator (Millipore). For crystallography, $CyaB_{220–416}$ was subjected to size-exclusion chromatography in 20 mM Tris-HCl, pH 7, 100 mM NaCl, 2 mM DTT on a Superose-12 column. Pure fractions were pooled, concentrated, frozen in aliquots in liquid nitrogen, and stored at 80°C. Slr1991 residues 120–337 were expressed and purified as previously described [37].

Activity assays

Regular AC assays were done in a 30 μl volume of 20 mM Tris-HCl, pH 7, 100 mM NaCl, 5 mM ATP, 10 mM $MgCl_2$, and 0.5–2.25 μg purified CyaB protein. Samples were incubated at 30°C for 30 min, and cAMP concentrations determined by using an ELISA (Biomol) according to the manufacturers' instructions. Experiments were done in duplicates and results shown are representatives of at least three repetitions. AC assays to assess the response to CO_2/HCO_3^- were performed as previously described [45]. Deviations from this setup are noted in the description of the respective results.

Crystallization, data collection and structure solution

For crystallization of $CyaB_{220–416}$, drops were mixed from 0.8 μl protein (10 mg/ml) and 0.8 μl reservoir (0.1 M MES, pH 6.5 and 12 % w/v PEG 20,000), equilibrated against 0.4 ml reservoir at 20°C. Crystals were transferred to cryo-protection solution containing reservoir components plus 25 % glycerol. A complete diffraction data set of a CyaB220–416 crystal of space group P2 was collected at 100 K at Swiss Light Source beamline X10SA. Indexing, scaling, and merging were done with XDS [53]. The structure of $CyaB_{220–416}$ was solved by using Patterson search techniques with PHASER [54], using the AC CyaC homodimer [38] (PDB ID 1WC1) as search model. For completing the model, manual model building in Coot [55] was alternated with positional and individual B-factor refinement with REFMAC [56]. Close to convergence of the refinement, solvent atoms and a glycerol molecule were included. The refined structure was analyzed by using Coot and ProCheck [57], and structural figures were generated with PyMOL (www.pymol.org) if not stated otherwise.

Supplementary Material

Refer to Web version on PubMed Central for supplementary material.

Acknowledgments

We thank Dr. Christine Schlicker, our colleagues from the Max Planck Institute for Molecular Physiology (Dortmund, Germany), and the beamline staff of X10SA at the Swiss Light Source, Villigen, Switzerland, for technical help. This work was supported by grant ST1701/7 of Deutsche Forschungsgemeinschaft (to CSt), grant AI069116 from the National Institutes of Health (to MCW), and grants from the Leverhulme Trust and Wellcome Trust (to MJC).

Abbreviations used

AC	adenylyl cyclase
cAMP	cyclic adenosine 3′,5′-monophosphate
GC	guanylyl cyclase
MASE2	membrane associated sensor 2
RNAP	RNA polymerase
tmAC	transmembrane AC

References

1. Garau J, Gomez L. *Pseudomonas aeruginosa* pneumonia. Curr Opin Infect Dis. 2003; 16:135–43. [PubMed: 12734446]
2. Brennan AL, Geddes DM. Cystic fibrosis. Curr Opin Infect Dis. 2002; 15:175–82. [PubMed: 11964920]
3. Strateva T, Yordanov D. *Pseudomonas aeruginosa* - a phenomenon of bacterial resistance. J Med Microbiol. 2009; 58:1133–48. [PubMed: 19528173]
4. Gales AC, Jones RN, Turnidge J, Rennie R, Ramphal R. Characterization of *Pseudomonas aeruginosa* isolates: occurrence rates, antimicrobial susceptibility patterns, and molecular typing in the global SENTRY Antimicrobial Surveillance Program, 1997–1999. Clin Infect Dis. 2001; 32(Suppl 2):S146–55. [PubMed: 11320454]
5. West SE, Sample AK, Runyen-Janecky LJ. The *vfr* gene product, required for *Pseudomonas aeruginosa* exotoxin A and protease production, belongs to the cyclic AMP receptor protein family. J Bacteriol. 1994; 176:7532–42. [PubMed: 8002577]
6. Beatson SA, Whitchurch CB, Sargent JL, Levesque RC, Mattick JS. Differential regulation of twitching motility and elastase production by Vfr in *Pseudomonas aeruginosa*. J Bacteriol. 2002; 184:3605–13. [PubMed: 12057955]
7. Wolfgang MC, Lee VT, Gilmore ME, Lory S. Coordinate regulation of bacterial virulence genes by a novel adenylate cyclase-dependent signaling pathway. Dev Cell. 2003; 4:253–63. [PubMed: 12586068]
8. Barzu O, Danchin A. Adenylyl cyclases: a heterogeneous class of ATP-utilizing enzymes. Prog Nucleic Acid Res Mol Biol. 1994; 49:241–83. [PubMed: 7863008]
9. Kamenetsky M, Middelhaufe S, Bank EM, Levin LR, Buck J, Steegborn C. Molecular details of cAMP generation in mammalian cells: a tale of two systems. J Mol Biol. 2006; 362:623–39. [PubMed: 16934836]
10. Yahr TL, Vallis AJ, Hancock MK, Barbieri JT, Frank DW. ExoY, an adenylate cyclase secreted by the *Pseudomonas aeruginosa* type III system. Proc Natl Acad Sci U S A. 1998; 95:13899–904. [PubMed: 9811898]
11. Smith RS, Wolfgang MC, Lory S. An adenylate cyclase-controlled signaling network regulates *Pseudomonas aeruginosa* virulence in a mouse model of acute pneumonia. Infect Immun. 2004; 72:1677–84. [PubMed: 14977975]
12. Fulcher NB, Holliday PM, Klem E, Cann MJ, Wolfgang MC. The *Pseudomonas aeruginosa* Chp chemosensory system regulates intracellular cAMP levels by modulating adenylate cyclase activity. Mol Microbiol. 2010; 76:889–904. [PubMed: 20345659]
13. Linder JU, Schultz JE. The class III adenylyl cyclases: multi-purpose signalling modules. Cell Signal. 2003; 15:1081–9. [PubMed: 14575863]
14. Shenroy AR, Visweswariah SS. Class III nucleotide cyclases in bacteria and archaebacteria: lineage-specific expansion of adenylyl cyclases and a dearth of guanylyl cyclases. FEBS Lett. 2004; 561:11–21. [PubMed: 15043055]
15. Tesmer JJ, Sunahara RK, Gilman AG, Sprang SR. Crystal structure of the catalytic domains of adenylyl cyclase in a complex with Gsalpha. GTPgammaS. Science. 1997; 278:1907–16. [PubMed: 9417641]
16. Steegborn C, Litvin TN, Levin LR, Buck J, Wu H. Bicarbonate activation of adenylyl cyclase via promotion of catalytic active site closure and metal recruitment. Nat Struct Mol Biol. 2005; 12:32–7. [PubMed: 15619637]
17. Sinha SC, Sprang SR. Structures, mechanism, regulation and evolution of class III nucleotidyl cyclases. Rev Physiol Biochem Pharmacol. 2006; 157:105–40. [PubMed: 17236651]
18. Rauch A, Leipelt M, Russwurm M, Steegborn C. Crystal structure of the guanylyl cyclase Cya2. Proc Natl Acad Sci U S A. 2008; 105:15720–5. [PubMed: 18840690]
19. Tesmer JJ, Sunahara RK, Johnson RA, Gosselin G, Gilman AG, Sprang SR. Two-metal-Ion catalysis in adenylyl cyclase. Science. 1999; 285:756–60. [PubMed: 10427002]
20. Linder JU. Substrate selection by class III adenylyl cyclases and guanylyl cyclases. IUBMB Life. 2005; 57:797–803. [PubMed: 16393782]

21. Chen Y, Cann MJ, Litvin TN, Iourgenko V, Sinclair ML, Levin LR, Buck J. Soluble adenylyl cyclase as an evolutionarily conserved bicarbonate sensor. Science. 2000; 289:625–8. [PubMed: 10915626]
22. Cann MJ, Hammer A, Zhou J, Kanacher T. A defined subset of adenylyl cyclases is regulated by bicarbonate ion. J Biol Chem. 2003; 278:35033–8. [PubMed: 12829712]
23. Sunahara RK, Dessauer CW, Gilman AG. Complexity and diversity of mammalian adenylyl cyclases. Annu Rev Pharmacol Toxicol. 1996; 36:461–80. [PubMed: 8725398]
24. Nikolskaya AN, Mulkidjanian AY, Beech IB, Galperin MY. MASE1 and MASE2: two novel integral membrane sensory domains. J Mol Microbiol Biotechnol. 2003; 5:11–6. [PubMed: 12673057]
25. Hall RA, De Sordi L, Maccallum DM, Topal H, Eaton R, Bloor JW, Robinson GK, Levin LR, Buck J, Wang Y, Gow NA, Steegborn C, Muhlschlegel FA. CO(2) acts as a signalling molecule in populations of the fungal pathogen *Candidaalbicans*. PLoS Pathog. 2010; 6:e1001193. [PubMed: 21124988]
26. Schlicker C, Hall RA, Vullo D, Middelhaufe S, Gertz M, Supuran CT, Muhlschlegel FA, Steegborn C. Structure and inhibition of the CO_2-sensing carbonic anhydrase Can2 from the pathogenic fungus *Cryptococcus neoformans*. J Mol Biol. 2009; 385:1207–20. [PubMed: 19071134]
27. Hess KC, Jones BH, Marquez B, Chen Y, Ord TS, Kamenetsky M, Miyamoto C, Zippin JH, Kopf GS, Suarez SS, Levin LR, Williams CJ, Buck J, Moss SB. The “soluble” adenylyl cyclase in sperm mediates multiple signaling events required for fertilization. Dev Cell. 2005; 9:249–59. [PubMed: 16054031]
28. Dessauer CW, Tesmer JJ, Sprang SR, Gilman AG. The interactions of adenylate cyclases with P-site inhibitors. Trends Pharmacol Sci. 1999; 20:205–10. [PubMed: 10354616]
29. Schlicker C, Rauch A, Hess KC, Kachholz B, Levin LR, Buck J, Steegborn C. Structure-based development of novel adenylyl cyclase inhibitors. J Med Chem. 2008; 51:4456–64. [PubMed: 18630896]
30. Fuchs EL, Brutinel ED, Jones AK, Fulcher NB, Urbanowski ML, Yahr TL, Wolfgang MC. The *Pseudomonas aeruginosa* Vfr regulator controls global virulence factor expression through cyclic AMP-dependent and -independent mechanisms. J Bacteriol. 2010; 192:3553–64. [PubMed: 20494996]
31. Mougous JD, Gifford CA, Ramsdell TL, Mekalanos JJ. Threonine phosphorylation post-translationally regulates protein secretion in *Pseudomonas aeruginosa*. Nat Cell Biol. 2007; 9:797–803. [PubMed: 17558395]
32. Kuchma SL, Ballok AE, Merritt JH, Hammond JH, Lu W, Rabinowitz JD, O’Toole GA. Cyclic-di-GMP-mediated repression of swarming motility by *Pseudomonas aeruginosa*: the *pilY1* gene and its impact on surface-associated behaviors. J Bacteriol. 2010; 192:2950–64. [PubMed: 20233936]
33. Rietsch A, Mekalanos JJ. Metabolic regulation of type III secretion gene expression in *Pseudomonas aeruginosa*. Mol Microbiol. 2006; 59:807–20. [PubMed: 16420353]
34. Sinha SC, Wetterer M, Sprang SR, Schultz JE, Linder JU. Origin of asymmetry in adenylyl cyclases: structures of *Mycobacterium tuberculosis* Rv1900c. Embo J. 2005; 24:663–73. [PubMed: 15678099]
35. Dessauer CW, Tesmer JJ, Sprang SR, Gilman AG. Identification of a Gialpha binding site on type V adenylyl cyclase. J Biol Chem. 1998; 273:25831–9. [PubMed: 9748257]
36. Mou TC, Masada N, Cooper DM, Sprang SR. Structural basis for inhibition of mammalian adenylyl cyclase by calcium. Biochemistry. 2009; 48:3387–97. [PubMed: 19243146]
37. Hammer A, Hodgson DR, Cann MJ. Regulation of prokaryotic adenylyl cyclases by CO_2. Biochem J. 2006; 396:215–8. [PubMed: 16573521]
38. Steegborn C, Litvin TN, Hess KC, Capper AB, Taussig R, Buck J, Levin LR, Wu H. A novel mechanism for adenylyl cyclase inhibition from the crystal structure of its complex with catechol estrogen. J Biol Chem. 2005; 280:31754–9. [PubMed: 16002394]
39. Linder JU, Schultz JE. Versatility of signal transduction encoded in dimeric adenylyl cyclases. Curr Opin Struct Biol. 2008; 18:667–72. [PubMed: 19054664]

40. Inclan YF, Huseby MJ, Engel JN. FimL regulates cAMP synthesis in *Pseudomonas aeruginosa*. PLoS One. 2011; 6:e15867. [PubMed: 21264306]
41. Chiang P, Habash M, Burrows LL. Disparate subcellular localization patterns of *Pseudomonas aeruginosa* Type IV pilus ATPases involved in twitching motility. J Bacteriol. 2005; 187:829–39. [PubMed: 15659660]
42. DeLange PA, Collins TL, Pierce GE, Robinson JB. PilJ localizes to cell poles and is required for type IV pilus extension in *Pseudomonas aeruginosa*. Curr Microbiol. 2007; 55:389–95. [PubMed: 17713814]
43. Kasahara M, Yashiro K, Sakamoto T, Ohmori M. The *Spirulina platensis* adenylate cyclase gene, *cyaC*, encodes a novel signal transduction protein. Plant Cell Physiol. 1997; 38:828–36. [PubMed: 9297847]
44. Kanchan K, Linder J, Winkler K, Hantke K, Schultz A, Schultz JE. Transmembrane signaling in chimeras of the *Escherichia coli* aspartate and serine chemotaxis receptors and bacterial class III adenylyl cyclases. J Biol Chem. 2010; 285:2090–9. [PubMed: 19923210]
45. Townsend PD, Holliday PM, Fenyk S, Hess KC, Gray MA, Hodgson DR, Cann MJ. Stimulation of mammalian G-protein-responsive adenylyl cyclases by carbon dioxide. J Biol Chem. 2009; 284:784–91. [PubMed: 19008230]
46. Mogensen EG, Janbon G, Chaloupka J, Steegborn C, Fu MS, Moyrand F, Klengel T, Pearson DS, Geeves MA, Buck J, Levin LR, Muhlschlegel FA. *Cryptococcus neoformans* senses CO_2 through the carbonic anhydrase Can2 and the adenylyl cyclase Cac1. Eukaryot Cell. 2006; 5:103–11. [PubMed: 16400172]
47. Klengel T, Liang WJ, Chaloupka J, Ruoff C, Schroppel K, Naglik JR, Eckert SE, Mogensen EG, Haynes K, Tuite MF, Levin LR, Buck J, Muhlschlegel FA. Fungal adenylyl cyclase integrates CO_2 sensing with cAMP signaling and virulence. Curr Biol. 2005; 15:2021–6. [PubMed: 16303561]
48. Innocenti A, Muhlschlegel FA, Hall RA, Steegborn C, Scozzafava A, Supuran CT. Carbonic anhydrase inhibitors: inhibition of the beta-class enzymes from the fungal pathogens *Candida albicans* and *Cryptococcus neoformans* with simple anions. Bioorg Med Chem Lett. 2008; 18:5066–70. [PubMed: 18723348]
49. Pierre S, Eschenhagen T, Geisslinger G, Scholich K. Capturing adenylyl cyclases as potential drug targets. Nat Rev Drug Discov. 2009; 8:321–35. [PubMed: 19337273]
50. Suryanarayana S, Gottle M, Hubner M, Gille A, Mou TC, Sprang SR, Richter M, Seifert R. Differential inhibition of various adenylyl cyclase isoforms and soluble guanylyl cyclase by 2′,3′-O-(2,4,6-trinitrophenyl)-substituted nucleoside 5′-triphosphates. J Pharmacol Exp Ther. 2009; 330:687–95. [PubMed: 19494187]
51. Furste JP, Pansegrau W, Frank R, Blocker H, Scholz P, Bagdasarian M, Lanka E. Molecular cloning of the plasmid RP4 primase region in a multi-host-range tacP expression vector. Gene. 1986; 48:119–31. [PubMed: 3549457]
52. Boyd JM, Lory S. Dual function of PilS during transcriptional activation of the *Pseudomonas aeruginosa* pilin subunit gene. J Bacteriol. 1996; 178:831–9. [PubMed: 8550520]
53. Kabsch W. Automatic processing of rotation diffraction data from crystals of initially unknown symmetry and cell constants. J Appl Cryst. 1993; 26:795–800.
54. McCoy AJ, Grosse-Kunstleve RW, Storoni LC, Read RJ. Likelihood-enhanced fast translation functions. Acta Crystallogr D Biol Crystallogr. 2005; 61:458–64. [PubMed: 15805601]
55. Emsley P, Cowtan K. Coot: model-building tools for molecular graphics. Acta Crystallogr D Biol Crystallogr. 2004; 60:2126–32. [PubMed: 15572765]
56. Murshudov GN, Vagin AA, Dodson EJ. Refinement of macromolecular structures by the maximum-likelihood method. Acta Crystallogr D Biol Crystallogr. 1997; 53:240–55. [PubMed: 15299926]
57. Laskowski RA, Moss DS, Thornton JM. Main-chain bond lengths and bond angles in protein structures. J Mol Biol. 1993; 231:1049–67. [PubMed: 8515464]

- Characterization of CyaB, an adenylyl cyclase regulating *P. aeruginosa* virulence
- The MASE2 domain of CyaB acts as membrane anchor and influences cyclase activity
- Residues involved in CyaB regulation identified using a random mutagenesis screen
- A CyaB catalytic core crystal structure reveals location and function of the residues
- Modulation of CyaB through CO2/HCO_3^- and known AC inhibitors

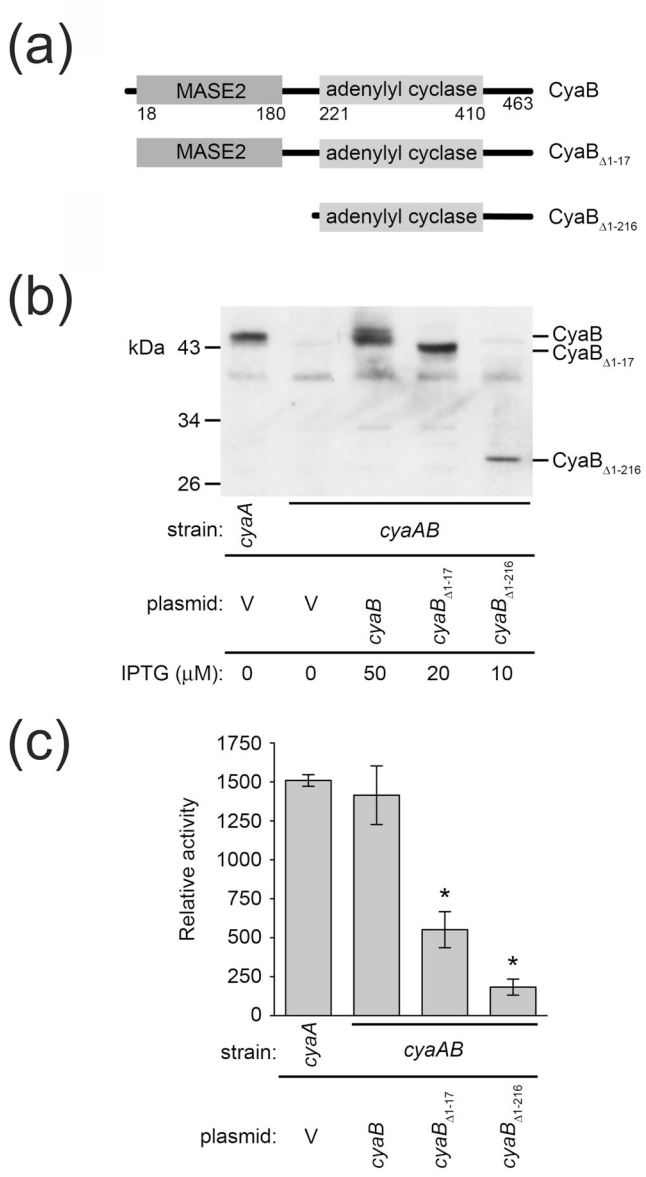

Figure 1. Regions outside the CyaB catalytic domain affect activity *in vivo*

(a) Diagram of the domain organization of native CyaB and the truncated CyaB proteins $CyaB_{\Delta 1–17}$ and $CyaB_{\Delta 1–216}$. The N-terminal MASE2 domain (PF05230) contains six predicted transmembrane α-helices (not shown); the C-terminus contains a guanylate_cyc (PF00211) domain present in Class III GCs and ACs. Relevant amino acid positions are indicated. (b) Immunoblot of whole-cell lysates from *cyaA* or *cyaAB* mutants carrying either an empty vector (V), pMMBV2 expressing *cyaB* or $cyaB_{\Delta 1–17}$, or pMMB expressing $cyaB_{\Delta 1–216}$, probed with anti-CyaB antibody. Expression of *cyaB* or $cyaB_{\Delta 1–17}$ from pMMBV2 at 50 or 20 μM IPTG, respectively, yielded a level of CyaB approximately equivalent to that of the wild-type strain; expression of $cyaB_{\Delta 1–216}$ from the pMMB plasmid, which has higher *tac* promoter activity, required 10 μM IPTG. Samples were normalized based on bacterial number. Molecular weight size standards are indicated. (c) cAMP reporter activity (corrected for CyaB protein levels) in the *cyaA* or *cyaAB* mutants carrying either an empty vector (V), pMMBV2 expressing *cyaB* or $cyaB_{\Delta 1–17}$, or pMMB expressing $cyaB_{\Delta 1–216}$. All strains contained the chromosomal *lac*P1Δ*lacI-lacZ* reporter and

were grown to mid-exponential growth phase with amount of IPTG indicated above. Equivalent samples were assayed for β-galactosidase activity and analyzed by quantitative immunoblot. CyaB levels were normalized based on the *cyaA* mutant carrying V and used to calculate relative activity. Bars represent the mean ± SEM of at least three independent experiments. The asterisk (*) indicates that the values for the indicated strains were significantly different ($P < 0.0001$) when compared pairwise to the value for the *cyaA* mutant carrying V.

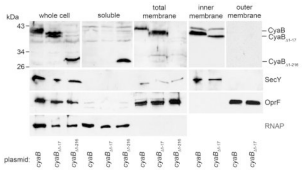

Figure 2. The MASE2 domain is required for CyaB membrane localization

Bacterial cell fractions from PAK*cyaAB* expressing wild-type CyaB or $CyaB_{\Delta 1–17}$ from pMMBV2, or $CyaB_{\Delta 1–216}$ from pMMB. Strains were grown to mid-exponential growth phase with 50 (CyaB), 20 ($CyaB_{\Delta 1–17}$) or 10 ($CyaB_{\Delta 1–216}$) μM IPTG. Whole-cell lysates, soluble (cytoplasmic-periplasmic) fractions and membrane (total, inner, and outer) fractions were subjected to SDS-PAGE and probed with antibody specific for CyaB, SecY, OprF or RNAP β subunit. For CyaB immunoblots, 15 μl of whole-cell lysate or 15 μg of fractionated protein was loaded; for all other immunoblots, 2μl of whole-cell lysate or 2 μg of fractionated protein was loaded. RNAP β subunit (~150 kDa) served as a control for cytoplasmic localization; SecY (~50 kDa) and OprF (~34 kDa) served as inner and outer membrane fraction markers, respectively. Molecular weight size standards are indicated. Samples were fractionated at the same time, but were immunoblotted on different days. The immunoblots are representative of at least two independent experiments.

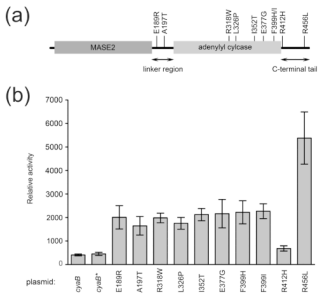

Figure 3. Analysis of CyaB mutants with increased enzyme activity

(a) Diagram indicating the site of CyaB missense mutations obtained in the screen for elevated cAMP-dependent reporter activity. (b) cAMP reporter activity (corrected for CyaB protein levels) in the *cyaAB* mutant carrying pMMBV2 expressing either *cyaB*, a *cyaB* wild-type clone from the screening strain (*cyaB**), or the indicated *cyaB* mutant. All strains contained the chromosomal *lac*P1Δ*lacI-lacZ* reporter. Strains were grown to mid-exponential growth phase in LB with 5 mM NaCl (low salt) and 50 μM IPTG. Equivalent samples were assayed for β-galactosidase activity and analyzed by quantitative immunoblot. CyaB levels were normalized based on the *cyaAB* mutant carrying pMMBV2-*cyaB* and used to calculate relative activity. Bars represent the mean ± SEM of three independent experiments. Values for all CyaB mutants (except R412H)) were significantly different ($P \leq 0.043$) when compared pairwise to the value for the *cyaAB* mutant carrying pMMBV2-*cyaB*.

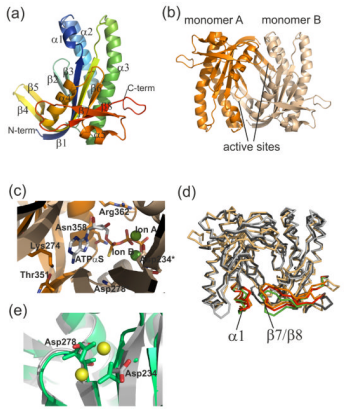

Figure 4. Crystal structure of the CyaB catalytic domain

(a) Overall structure of the CyaB monomer with labelled secondary structure elements. The connectivity is indicated through rainbow coloring from blue (N-terminus) to red (C-terminus). (b) Overall structure of the catalytic CyaB homodimer, with chain A and B colored orange and light orange, respectively. The locations of the two active sites at the dimer interface, derived through comparison to other Class III ACs, are indicated. (c) Active site of CyaB, with ATPαS and the two divalent ions A and B modelled into the substrate binding pocket through overlay with a CyaC/ATPαS complex (PDB ID 1WC1). Conserved Class IIIb catalytic residues are shown as sticks and labelled (* indicates residues from monomer B). (d) Comparison of CyaB (light orange) with the open (light grey; PDB ID 1WC0) and closed (dark grey; 1WC1) conformations of CyaC. The structural elements showing major movements during catalysis are highlighted (CyaB: dark orange; CyaC open: green; CyaC closed: red) and labelled. (e) Close view of the empty CyaB (grey) active site overlaid with the CyaC/ATPαS complex (green; PDB ID 1WC1). The magnesium ions from the CyaC structure are shown as yellow spheres, and the Asp of CyaB are labelled and colored according to atom type. The Asp side chains of CyaB are partially and fully rotated, respectively, opening up the ion binding sites. In CyaC, in contrast, the Asp side chains are oriented toward the ions and coordinate each magnesium with one oxygen atom.

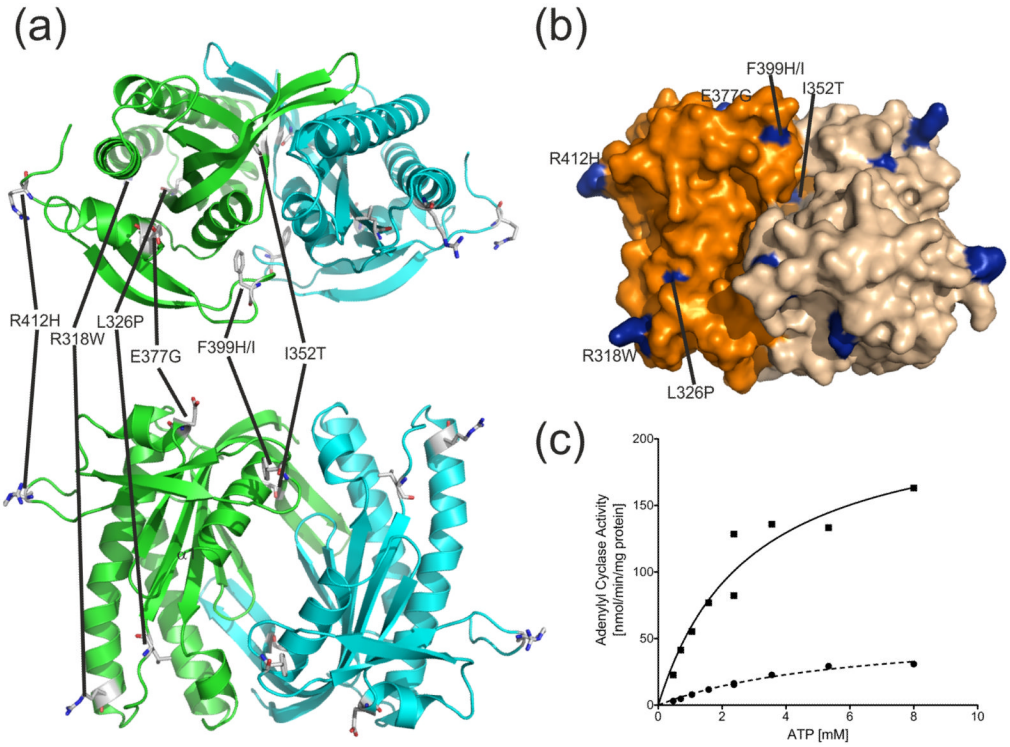

Figure 5. Structural analysis of residues involved in CyaB regulation

(a) Activating mutations identified in a genetic screen are shown as sticks in the front and top views of the CyaB crystal structure, and (b) as blue patches on the surface of the structure. Amino acids at these positions and the substituting amino acid are indicated with one-letter codes. (c) Comparison of specific activities of $CyaB_{220–416}$ wildtype (●) and the $CyaB_{220–416}$-Leu326Pro mutant (■) determined at 10 mM Mn^{2+} and increasing ATP concentrations.

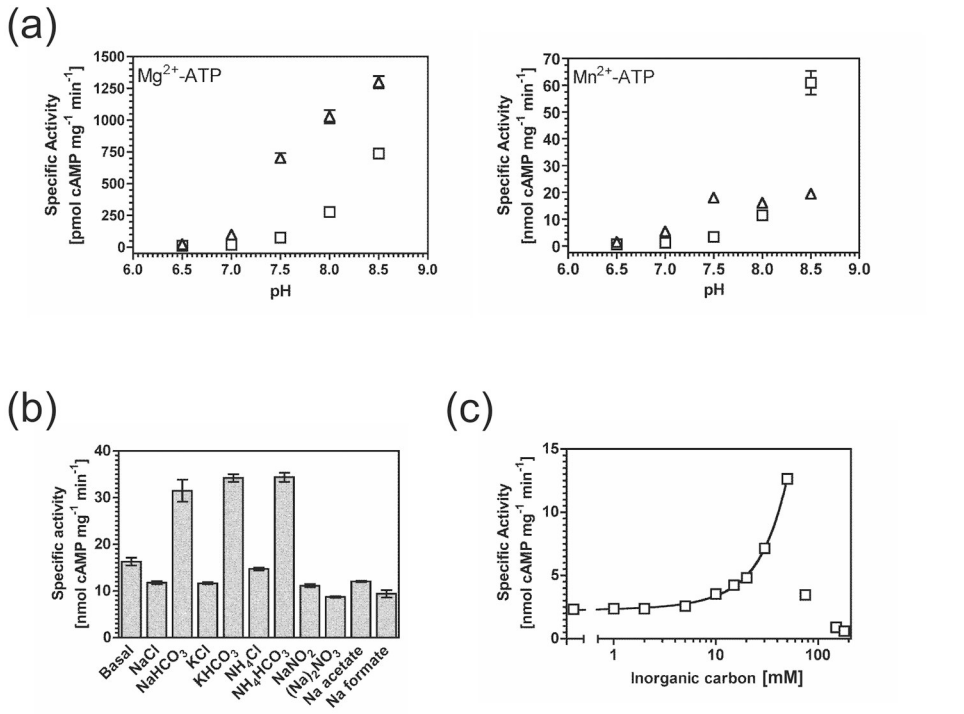

Figure 6. Regulation of CyaB by bicarbonate

(a) 0.17 μM (Mn^{2+}-ATP) or 13.7 μM (Mg^{2+}-ATP) $CyaB_{217–463}$ was assayed at varying pH at 40°C with 0.2 mM (Mn^{2+}-ATP) or 1 mM (Mg^{2+}-ATP) substrate in the presence of 20 mM NaCl (□) or $NaHCO_3^-$ (Δ). (b) 0.17 μM $CyaB_{217–463}$ was assayed at pH 7.5, with 30 mM salt at 40°C and 0.2 mM Mn^{2+}-ATP as substrate. (c) 0.17 μM $CyaB_{217–463}$ was assayed at pH 7.5 and 40°C with varying concentrations of $NaHCO_3$ and NaCl to maintain a constant 180 mM total salt concentration, and 0.2 mM Mn^{2+}-ATP as substrate. The drop of activity beyond 50 mM $NaHCO_3$ is likely a precipitation artefact typically observed for Mn^{2+}at high $NaHCO_3$ concentrations.

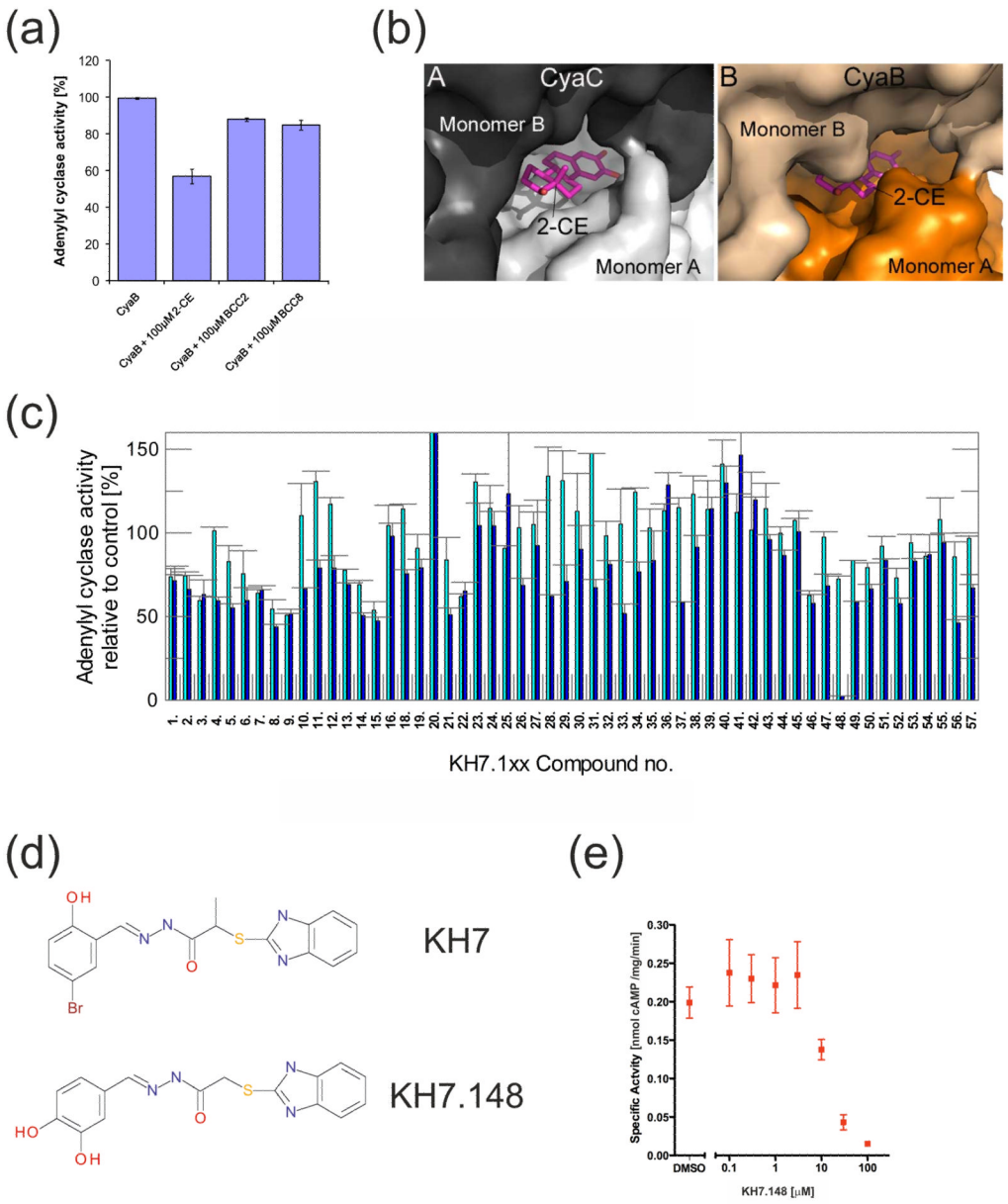

Figure 7. Regulation of CyaB by small molecule drugs

(a) Inhibition of CyaB AC activity by 100 μM 2-CE, BCC2, and BCC8, respectively. (b) Comparison of the CE binding sites of CyaC (A) and CyaB (B). The inhibitor was put into the corresponding CyaB site based on an overlay with the crystal structure of the CyaC/CE complex (PDB ID 2BW7). (c) Screening for CyaB inhibitors by testing a library of KH7 derivatives. AC assays were performed with 1 mM ATP in the presence of 10 μM (blue bars) or 100 μM (red bars) drug. (d) Chemical structures of KH7 and KH7.148. (e) Dose-response curve for inhibition of CyaB by KH7.148, indicating an IC_{50} of ~10 μM.

Table I

CyaB mutants with altered cAMP reporter activity.

mutation*	number of clones
E189R	8
E377G	7
L326P	3
F399I	3
R318W	2
A197T	1
I352T	1
F399H	1
R412H	1
R456H	1

* amino acid position

Table II

Crystallographic data and refinement statistics

	CyaB
Space group	P2
Unit cell constants	a = 51.4 Å, b = 36.3 Å, c = 94.8 Å; β = 98.76°
Resolution limit	1.5 Å
Unique reflections	50946
$\langle I / \sigma \rangle$ *(a)*	20.6 (4.6)
Completeness *(a)*	91.2 % (61.4 %)
R_{merge} *(a)*	5.4 % (36.4 %)
Refinement resolution	47.8 – 1.5 Å
Total reflections used	48397
R_{cryst} / R_{free} *(b)*	18.6 % / 23.0 %
Atoms: protein / solvent + glycerol	3054 / 323
R.m.s.d. bond lengths	0.028 Å
R.m.s.d. Bond angles	2.4°
Average B-factor: protein / solvent + glycerol	20.8 $Å^2$ / 32.1 $Å^2$

(a) Numbers in parentheses are for the outermost shell (1.5–1.6 Å)

(b) R_{free} was calculated from 5 % of measured reflections omitted from refinement.